European Control Conference, ECC 2015. 15-17 July 2015, Linz, Austria. pp660-665
10.1109/ECC.2015.7330617

Cost Functions for Degradation Control of Electric Motors in Electric Vehicles

Lilantha Samaranayake and Stefano Longo

Abstract— **This paper introduces a novel set of electric motor degradation cost functions based on energy usage, energy loss and work output, against their continuous operation rated values recommended by the manufacturer. Unlike conventional electric motor degradation indicators such as the bearing life and insulation life based service factors, these cost functions account for the quantified time in the degradation process. The cost functions are evaluated throughout the operational life of the motor using real-time measurements. Hence, they give a very accurate indication, which may be adapted for online controller tuning. This solid establishment of a degradation cost function also enables the system designer to give the user a choice between performance and degradation minimization.**

The proposed cost function scheme has experimentally been verified using a hardware-in-the-loop electric powertrain test-rig where standard drive cycles are used to conduct the experiments. The experimental results reveal that the degradation cost functions Cumulative Input Energy Ratio (CIER), Cumulative Loss Ratio (CLR) and Cumulative Work Ratio (CWR) accurately represent the electric motor degradation both qualitatively and quantitatively.

I. INTRODUCTION

Electric motor has been the industrial work horse over the past century. During the last few decades it has been gaining recognition as a greener and more efficient alternative to the internal combustion engine in the transportation sector. Nowadays it very common to use electric motors in different types of electric vehicles such as plug-in electric vehicles, series hybrid electric vehicles, parallel hybrid electric vehicles and combined hybrid electric vehicles [1] - [3].

In the electric vehicle design, various optimization methods are used to ensure optimum utilization of various device and component capabilities to the advantage of the vehicle construction and the benefits to its users. During the operational life of the electric vehicle, the energy management system makes sure the limited energy on-board is utilised optimally to ensure higher range while delivering the user desired performance [4] - [6].

As any natural creature born or any artificial object created, electric motors in electric vehicles also deteriorate, degrade and expire. Despite that, in the process industry applications, the electric motor is considered to be one of the most rugged elements in the mechanical power supply chain because its operation is confined to a limited operating regions which are usually around the most efficient, rated operating points.

Lilantha Samaranayake and Stefano Longo are with the Centre for Automotive Engineering and Technology, School of Aerospace Transport and Manufacturing, Cranfield University, Bedfordshire, United Kingdom MK43 0AL l.b.samaranayake,s.longo@cranfield.ac.uk

As any natural creature born or any artificial object created, electric motors in electric vehicles also deteriorate, degrade and expire. Despite that, in the process industry applications, the electric motor is considered to be one of the most rugged elements in the mechanical power supply chain because its operation is confined to a limited operating regions which are usually around the most efficient, rated operating points. Therefore, the component level degradation indicators such as bearing life based on the number of revolutions turned, or the materials level degradation indicators such as the service factors depending on the over temperature conditions detected during the operation of the motor, have been used to assess the degradation and estimate remaining useful life [7] - [15].

With the paradigm shift of electric motors role as a prime mover in the electric vehicles, the motor control has come across new challenges as it needs to be operated in almost every operating point in the characteristic curve, subjected to thermal, battery and power electronic limitations. New designs with wider high efficiency regions have contributed substantially to ease the challenges. The new designs use to specify two separate characteristic curves, one for the continuous operation where the efficiency will be higher and degradation will be lower and another for the peak value operations, where the degradation will be higher and not recommended to operate more than a specified time such as 60 s at a time to avoid reaching harmful temperatures [16]. This approach tremendously helps to keep both the weight and the cost lower. But on the other hand, it can be interpreted as undersized design because it can not deliver peak torque throughout its operational life continuously. This leads to accelerated degradation of the electric motor not by its individual components such as bearings or by its material such as insulation, but as a system which become unable to deliver the power demand. The situation becomes worse when inexpensive materials are substituted as a means of reducing the cost. For example, rare earth materials are being replaced with ferrite materials for magnets in permanent magnet motors [17] - [18].

Hence the above new specifications on characteristic curves and restrictions on operating times in certain regions, impose new challenges to the assessment of the degradation. Therefore the bearing life and insulation life are not sufficient simply because they only account for quantified amplitude but do not account for the duration. In addition, their combined effect together with other possible modes of degradation contributes to the complete degradation of the motor, which is observed as a reduction in working capability

(c) 2015 IEEE. Personal use of this material is permitted. Permission from IEEE must be obtained for all other users, including reprinting/ republishing this material for advertising or promotional purposes, creating new collective works for resale or redistribution to servers or lists, or reuse of any copyrighted components of this work in other works.

[20]. A typical manufacturer datasheet is given in Fig. 1 [16] to exemplify the existence of two characteristic curves and time restrictions on certain operating points. This paper

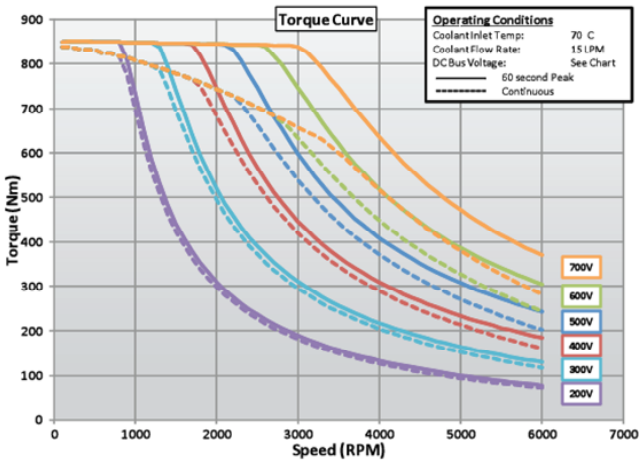

Fig. 1. Typical manufacturer data showing the continuous operation characteristic curve (dotted line) and peak operation characteristic curve (continuous line) with 60 s time limit.

introduces a novel set of motor degradation cost functions based on energy usage, energy loss and work output, which do account for quantified time in the degradation. They quantify the excess energy usage, excess energy loss and excess work output while operating at points other than the continuous operation characteristic curve.

The control engineers can use these cost functions in deriving motor control schemes, where it takes real-time motor degradation into account in a more realistic and a practical manner. It also enables to offer advanced control schemes, where closed loop performance (J_{CL}) versus degradation (J_{DEG}) can be optimally tuned online as per user preference, where the total cost function can be given for $0 \leq \alpha \leq 1$ as

$$J = \alpha J_{CL} + (1 - \alpha) J_{DEG}.$$

The paper is organized as follows. Section II presents a set of motor degradation cost functions based on energy usage, energy loss and work output. Section III describes the experimental followed to validate the cost functions using standard drivetrain hardware. Section IV presents the experimental results followed by a discussion and Section V concludes the paper with an outline of the future work.

II. The Motor Degradation Cost Functions

The concept of degradation assessment presented in this paper has been developed based on a natural scenario. The philosophy is that, every living creature and every physical natural or artificial object has a finite life time that gets defined at its origin. There is hardly any chance for this original life time to get prolonged, but instead it may get shortened depending on the life style for a living creature and depending on how it is being used and under the conditions of the environment for physical objects [19]. Though electric motors in electric vehicles as well as the electric vehicles themselves are man-made objects, they must undergo the same natural scenario. Obviously, their useful life will come to an end on one day. But from an instant between the origin and the expire, the remaining useful life of them will be influenced by how they have been used and under what environmental conditions they have been operated (temperature, humidity, vibration, ventilation, etc.,). The electric motors are designed for some rated speed, torque and power P_{rated} on the continuous operation of the characteristic curve. Depending on the design, manufacturing procedure, quality of the raw materials and the technology, the manufacturer recommends a useful life time t_{life}. The t_{life} is influenced by how often the motor is operated beyond the continuous operation of the characteristic curve subjected to the maximum limitations defined by the peak operation characteristic curve. For an electric motor, the entire amount of work that it can be done during its manufacturer recommended useful life time can be evaluated by:

$$W_{rated} = \int_0^{t_{life}} P_{rated} dt \tag{1}$$

During the useful life time, the motors will be operated many times delivering non-zero power. The work done by the motor in it's i^{th} continuous operation which takes place from time $t_{initial_i}$ to t_{final_i} can be given by

$$W_{output_i} = \int_{t_{initial_i}}^{t_{final_i}} P_{output_i}(t)\, dt, \tag{2}$$

where the instantaneous output power is given in terms of the instantaneous shaft torque $\tau_{output_i}(t)$ and the speed $\omega_{output_i}(t)$ as

$$P_{output_i}(t) = \tau_{output_i}(t)\, \omega_{output_i}(t). \tag{3}$$

Due to non-ideal conditions, when converting electrical energy to mechanical energy using motors and also during energy transfer back to the source during regeneration in torque reversal, it involves several types of energy losses. The energy lost during the above i^{th} operation can be given by

$$W_{losses_i} = \int_{t_{initial_i}}^{t_{final_i}} P_{losses_i}(t)\, dt, \tag{4}$$

where the power loss of a motor in general consists of the resistive losses in the windings due to current, i.e., copper loss P_{Cu}, flux dependant iron losses P_{Fe} (Hysteresis losses and Eddy current losses), dynamic friction, windage and other losses accounting for mechanical losses P_{Mech} related as

$$P_{losses_i}(t) = P_{Cu_i}(t) + P_{Fe_i}(t) + P_{Mech_i}(t). \tag{5}$$

These losses will not remain constant. Depending on how the motor is operated, maintained, environmental factors and the age, the losses will vary. Therefore, taking all the losses in to account, for N number of operations of the motor, the cumulative work W_{actual} done by the motor will be

$$W_{actual} = \Sigma_{i=1}^{N} W_{output_i} + W_{losses_i}. \tag{6}$$

It is interesting to note here that the ratio $\frac{W_{actual}}{W_{rated}}$ (< 1) represents the fraction of the working capability of the motor which has already been used. Therefore

$$RUL = 1 - \frac{W_{actual}}{W_{rated}} \tag{7}$$

represents the Remaining Useful Life (RUL) of the motor. Hence it is straight forward to calculate the RUL online using time integrals of instantaneous input power to the motor. Thus it is a very flexible approach which can also be adapted in an existing setup with minimum modifications. In order to identify the degree of degradation, this paper proposes three degradation cost functions (J_{DEG}), namely; Cumulative Work Ratio (CWR), Cumulative Loss Ratio (CLR) and Cumulative Input Energy Ratio (CIER), i.e.,

$$J_{DEG} \in [CWR, CLR, CIER]$$

A. Cumulative Work Ratio

The Work Ratio for the i^{th} operation of the motor is defined as

$$WR_i = \frac{\int_{t_{inititial_i}}^{t_{final_i}} P_{output_i}(t)\,dt}{\int_{t_{inititial_i}}^{t_{final_i}} P_{rated} dt}, \tag{8}$$

where it compares the actual work done by the motor during the drive cycle taking in to account the instantaneous output torque and output speed against the work done in delivering rated power during the same interval. Ideally the Work Ratio should be less than or equal to unity. However, if it goes beyond unity, may be as a part of the drive cycle, it is considered to be over burdening the motor. The latter over burdening will eventually be contributed to degrade the motor and reduce the life time. In order to integrate the history of operations of the motor, the Work Ratio concept is extended to Cumulative Work Ratio (CWR) as

$$CWR = \frac{\Sigma_{i=1}^{N} \int_{t_{inititial_i}}^{t_{final_i}} P_{output_i}(t)\,dt}{\int_0^{t_{life}} P_{rated} dt}, \tag{9}$$

where it compares the total work delivered in N driving cycles against the total amount of work the motor is supposed to deliver during its entire life time, which is typically for 30,000 hours for a 15 year electric vehicle design. If the motor undergoes frequent overburdening, CWR will soon reach unity. The more degrade the motor, the closer CWR to unity. Hence the quantified effects over the time are taken into account in the degradation cost function.

B. Cumulative Loss Ratio

The Loss Ratio (LR) and Cumulative Loss Ratio have been formulated based on the losses that the motor will encounter in delivering the work output. With η being the efficiency, the LR for the i^{th} operation of the motor will be defined as

$$LR_i = \frac{\int_{t_{inititial_i}}^{t_{final_i}} \left(P_{input_i}(t) - P_{output_i}(t)\right) dt}{\int_{t_{inititial_i}}^{t_{final_i}} \left(\frac{1}{\eta} - 1\right) P_{rated} dt}. \tag{10}$$

Instead of calculating losses separately, which needs to access many extra variables, it is assumed that the difference between input and output power is the power that is lost, which can be calculated using instantaneous input voltage, input current, output torque and output speed and integrating the power loss over the time. This lost energy is compared to the rated energy loss in case if the motor were delivering rated power at rated efficiency. In addition to degradation, an exceptionally high value of LR may also indicate a fault in the motor. The same concept is extended to indicate the total energy lost during the operation of N driving cycles against what the motor is supposed to loose during its entire life time by CLR, defined as

$$CLR = \frac{\Sigma_{i=1}^{N} \int_{t_{inititial_i}}^{t_{final_i}} \left(P_{input_i}(t) - P_{output_i}(t)\right) dt}{\int_0^{t_{life}} \left(\frac{1}{\eta} - 1\right) P_{rated} dt}. \tag{11}$$

C. Cumulative Input Energy Ratio

The Input Energy Ratio (IER) and CIER have been formulated based on the input electrical energy that the motor will consume in delivering the work output. The IER for the i^{th} operation of the motor will be defined as

$$IER_i = \frac{\int_{t_{inititial_i}}^{t_{final_i}} P_{input_i}(t)\,dt}{\int_{t_{inititial_i}}^{t_{final_i}} \left(\frac{1}{\eta}\right) P_{rated} dt}, \tag{12}$$

where the input power may be calculated using input voltage and input current. The total energy consumed is calculated by using the time integral of the instantaneous input power. It is compared against the energy that the motor is supposed to consume in delivering the rated output work. As in the previous two cases, this concept is also extended to include the history of operations by defining the Cumulative Input Energy Ratio as

$$CIER = \frac{\Sigma_{i=1}^{N} \int_{t_{inititial_i}}^{t_{final_i}} P_{input_i}(t)}{\int_0^{t_{life}} \left(\frac{1}{\eta}\right) P_{rated} dt}. \tag{13}$$

Hence unlike the bearing life and insulation life which only account for quantified amplitudes of operational aspects, the proposed set of motor degradation cost functions CIER, CLR and CWR, quantify the excess energy usage, excess energy loss and excess work output respectively while taking operating time also into account.

III. Experimental Verification of the Degradation Cost Functions

Since the cost functions derived above can be implemented using direct measurements, instead of a simulation study, they are experimentally verified directly. This section describes the experimental design and procedure followed for the verification of the Degradation Cost Functions.

A. Experimental design and procedure

The experiments are designed such that, given the same vehicle dynamics, road conditions, air resistance and other environment conditions such as surrounding air temperature,

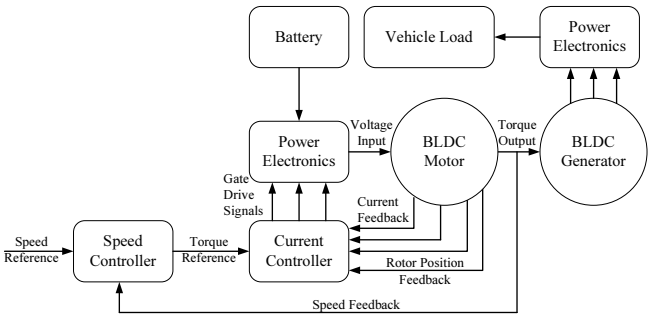

Fig. 2. Block diagram of the experimental test rig

Fig. 3. The experimental setup

humidity, ventilation, etc., the electric vehicle and hence the electric motors will be driven to follow the same drive cycle, but with different tracking accuracies. The integral absolute error (IAE) between the reference speed $r(t)$ and the actual speed $y(t)$, where

$$IAE = \int_0^\infty \mid r(t) - y(t) \mid dt \tag{14}$$

is taken as the measure of tracking accuracy. Three cases as

1) CASE1: Highly accurate, i.e., low IAE
2) CASE2: Moderately accurate, i.e., medium IAE
3) CASE3: Inaccurate, i.e., high IAE

have been used to create 3 scenarios, where all of them will generate similar torque profiles during the drive cycle, but with different speed profiles. Hence they will operate in 3 different torque-speed profiles in the characteristic curve of the motor, resulting in different degrees of degradation at the end. It is assumed that the motors used in the experiment are degraded equally at the beginning of the experiment. The experiments are carried out using urban centred New European Drive Cycle (NEDC) and motorway centred Assessment and Reliability of Transport Emission Models and Inventory Systems (ARTEMIS) drive cycle. Due to torque capability limitation of the motor, the torque demand of the ARTEMIS experiment has been scaled down purposely.

B. Experimental setup

The experimental setup consists of typical components of an electric vehicle drivetrain, namely the electric motor, the vehicle load and the dynamics, battery and the power electronics and the respective control. The vehicle dynamics are obtained by hardware-in the loop (HIL) control of a back-to-back connected motor working in the generator mode. The block diagram of the system is shown in Fig. 2. The motor is a Brush Less DC (BLDC) type with electronic commutation in the stator achieved through power electronics. The current controller converts the torque reference from the speed controller to the respective current references in each phase of the 3 phase windings and outputs the gate trigger signals to the power electronics block. The current controller employs nonlinear hysteresis type current comparators. The rotor position for the current controller is obtained from the Hall effect position sensors placed in the stator and the same rotor position signals are used to calculate the rotor speed of the motor.

The BLDC generator receives the vehicle dynamics from HIL system implemented using $dSPACE^{TM}$ system. Accordingly it generates electric power for an electric load (not shown in the figure) imposing the respective torque on the BLDC motor, which is the source of power for the generator. The $dSPACE^{TM}$ system consists of $DS1006$ processor with $dSPACE2013b$ real time operating system, $DS2202$ input-output card interfaced to the user through $ControlDesk^{TM}5.1$ proprietary software platform. The experimental setup is shown Fig. 3. The speed controller, receives the rotor speed of the BLDC motor indicating the vehicle speed. It is compared with the speed reference and the speed error is used to derive the current reference to the current controller. It resembles the operation of a driver of an actual vehicle and in this case the speed controller tries to follow a particular drive cycle introduced as the reference.

IV. Results and Discussion

The upper part of the Fig. 4 shows how NEDC is followed in each case. As was designed, the tracking accuracy is best in CASE 1 and worst in CASE 3. The lower part of the Fig. 4 shows the same load torque profile (vehicle demand) applied on the BLDC motor through the BLDC generator using the HIL setup. Fig. 5 shows the variation of CIER, CLR and CWR with IAE for the 3 cases. In the CASE 1, where the IAE is the lowest, the motor undergoes the highest torque-speed profile and consequently the degradation is expected to be the highest. Following the same argument, CASE 2 with intermediate IAE is expected to result in intermediate degradation and the CASE with highest IAE is expected to result in the lowest degradation. As seen in Fig. 5, this trend has been captured correctly by the degradation cost functions concerned. Fig. 6 shows the results of the experiment repeated with ARTEMIS drive cycle. Unlike in the previous case, here the difference in IAE between the CASES 1 and 2 is not narrow. With the

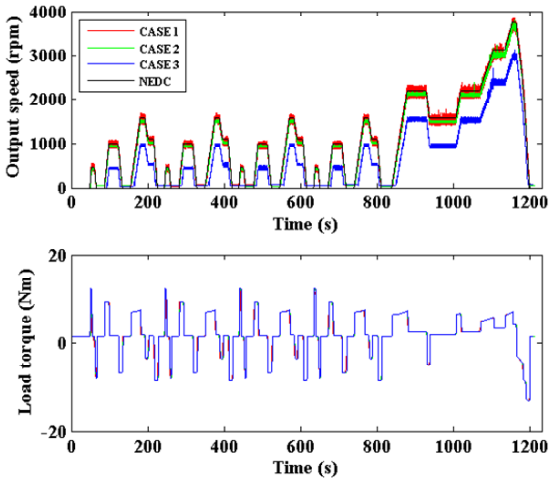

Fig. 4. Tracking NEDC

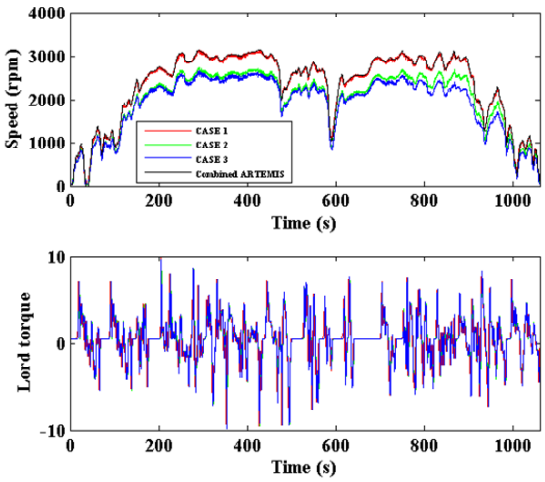

Fig. 6. Tracking ARTEMIS drive cycle

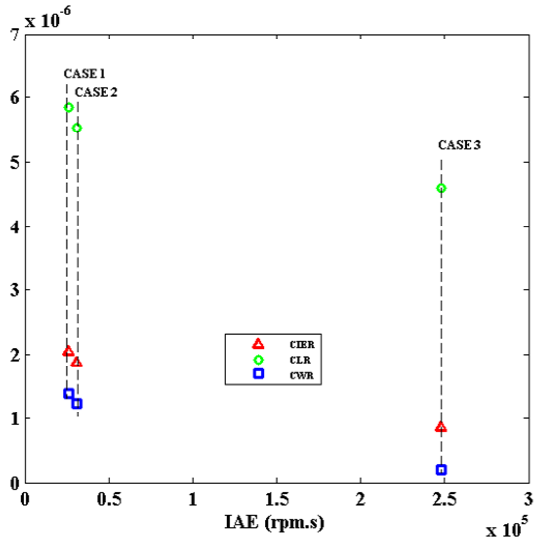

Fig. 5. Degradation Cost Functions with NEDC drive cycles

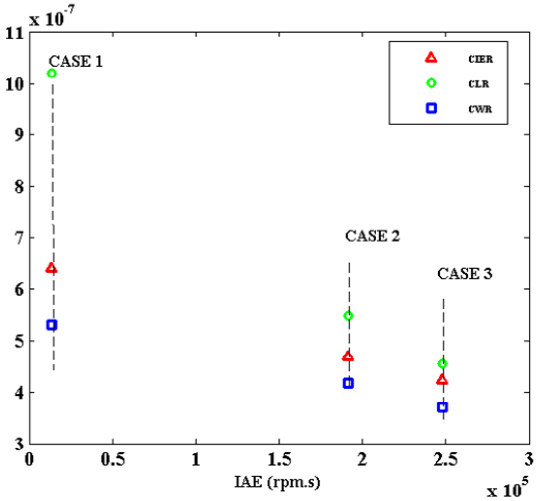

Fig. 7. Degradation Cost Functions with ARTEMIS drive cycles

ARTEMIS drive cycle too, in the CASE 1, where the IAE is the lowest, the motor undergoes the highest torque-speed profile and consequently the degradation is expected to be the highest. Following a similar argument, the other two CASES are expected result in intermediate and lower degradations respectively. As shown in Fig. 7, in the ARTEMIS drive cycle also, the latter scenario has been captured correctly by all 3 degradation cost functions. In addition, when comparing the results for NEDC and ARTEMIS drive cycles presented in Figs. 5 and 7 respectively, it is observed that the quantified degradation is higher in NEDC than that in ARTEMIS drive cycle, which is in contrary to the general understanding of the two drive cycles because the accelerations and the decelerations are higher in the ARTEMIS drive cycle.

The reason for this observation can be understood by analysing the operating points in the characteristic curve followed in each drive cycle against the efficiency map of the motor. As shown in Fig. 8, during NEDC, the motor undergoes a wider spectrum of speed profiles varying from very low speeds to very high speeds. In addition, the torque demand also varies between the two extreme ends of the motor capabilities. When referring the torque-speed profile during NEDC with the efficiency map of the motor shown in Fig. 9, it can be observed that, especially at low speeds, the motor operates in low efficient regions during a substantial number of instants as compared to the ARTEMIS cases. On the other hand, with the scaled down torque demand due to capacity limitation of the motor, during ARTEMIS drive cycle, the speed and torque spectrum are relatively narrower. Most importantly, as seen in the efficiency map, it operates in the highest efficiency regions throughout the drive cycle. Therefore the degradation should be lower. This has correctly been captured by the degradation cost functions as observed. Hence the degradation cost functions CIER, CLR and CWR

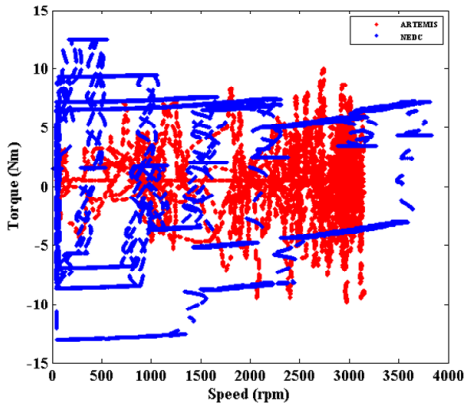

Fig. 8. Operating profiles followed during NEDC and ARTEMIS drive cycles

not only qualitatively, but also quantitatively characterize the degradations of the motor.

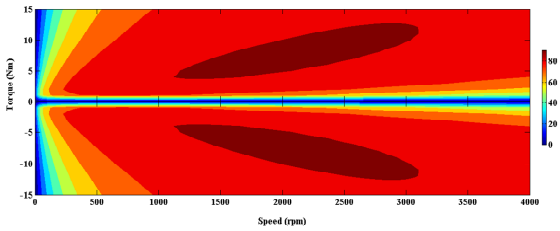

Fig. 9. Efficiency map of the motor used in the experiment

V. Conclusions and Future Work

A set of electric motor degradation cost functions based on energy usage, energy loss and work output, against their continuous operation rated values recommended by the manufacturer, have been derived and presented in this paper. A special emphasis has been paid to degradations of electric motors in electric vehicle applications, where the problem is expected to be severe in the near future. The validity of the proposed degradation cost functions have been experimentally verified using practical case studies deploying standard drive cycles. The logically derived expected trends in degradations are captured and represented correctly both quantitatively and qualitatively using CIER, CLR and CWR. Since the evaluation of cost function in real-time involves only basic measurements such as voltages, currents, torque and speed, it can readily be implemented in electric vehicle environments, using existing hardware available on board. This enables control engineers to implement real-time degradation minimization algorithms even on existing vehicle platforms.

The future work of this project will include optimal controller design using the proposed degradation cost functions to minimize degradation of electric motors in electric vehicles.

Acknowledgment

Authors acknowledge the financial support from EPSRC through FUTURE vehicles grant (EP/I038586/1) and Impact Acceleration Account grant (EP/K503927/1).

References

[1] N. Mutoh and S. Member, Driving and Braking Torque Distribution Methods for Front and Rear Wheel Independent Drive Type Electric Vehicles (FRID EVs) on Roads with Low Friction Coefficient, IEEE Trans. Ind. Electron., vol. 59, no. 10, pp. 3919,3933, 2011.

[2] S. S. Williamson, Efficiency analysis of hybrid electric vehicle (HEV) traction motor-inverter drive for varied driving load demands, 2008 Twenty-Third Annu. IEEE Appl. Power Electron. Conf. Expo., pp. 280,285, Feb. 2008.

[3] K. T. Chau, C. C. Chan, and C. Liu, Overview of permanent-magnet brushless drives for electric and hybrid electric vehicles, IEEE Trans. Ind. Electron., vol. 55, no. 6, pp. 2246 2257, 2008.

[4] J. Nerg, M. Rilla, V. Ruuskanen, J. Pyrhnen, and S. Ruotsalainen, Direct-driven interior magnet permanent-magnet synchronous motors for a full electric sports car, IEEE Trans. Ind. Electron., vol. 61, no. 8, pp. 4286,4294, 2014.

[5] C.-T. Pan and S.-M. Sue, A Linear Maximum Torque Per Ampere Control for IPMSM Drives Over Full-Speed Range, IEEE Trans. Energy Convers., vol. 20, no. 2, pp. 359 366, Jun. 2005.

[6] J. Lemmens, S. Member, P. Vanassche, J. Driesen, and S. Member, Optimal Control of Traction Motor Drives Under Electrothermal Constraints, IEEE J. Emerg. Sel. Top. Power Electron., vol. 2, no. 2, pp. 249,263, 2014.

[7] O. Winter, C. Kral, and E. Schmidt, Design and loss assessment of air cored axial flux permanent magnet machines, in Electric Machines and Drives Conference (IEMDC), 2013 IEEE International, pp. 602,606, 2013.

[8] T. Windisch and W. Hofmann, Loss minimization of an IPMSM drive using pre-calculated optimized current references, IECON 2011 - 37th Annu. Conf. IEEE Ind. Electron. Soc., pp. 4704,4709, Nov. 2011.

[9] S. Vohnout, D. Goodman, K. Harris, and J. Judkins, Electronic Prognostics System Implementation on Power Actuator Components, IEEE Aerosp. Conf. Proc., 2008.

[10] N. Kunst, J. Judkins, C. Lynn, and D. Goodman, Damage propagation analysis methodology for electromechanical actuator prognostics, IEEE Aerosp. Conf. Proc., 2009.

[11] H. G. Park, Y. J. Kwon, S. J. Hwang, H. D. Lee, and T. S. Kwon, A study for the estimation of temperature and thermal life of traction motor for commercial HEV, IEEE Vehicle Power and Propulsion Conf. Proc., 2012.

[12] R. K. Singleton, E. G. Strangas, and S. Aviyente, Time-frequency complexity based remaining useful life (RUL) estimation for bearing faults, 9th IEEE International Symposium on Diagnostics for Electric Machines, Power Electronics and Drives, Conf. Proc., 2013.

[13] P. Werynski, D. Roger, R. Corton, and J. F. Brudny, Proposition of a new method for in-service monitoring of the aging of stator winding insulation in AC motors, IEEE Trans. Energy Convers., vol. 21, no. 3, pp. 673,681, 2006.

[14] K. Cao, G. Wu, L. Zhou, X. Guo, K. Lei, and B. Gao, Insulation life-span models for electrical and thermal aging under continuous high square impulses voltage, Proc. IEEE Int. Conf. Prop. Appl. Dielectr. Mater., no. 1, pp. 285,288, 2009.

[15] N. Lahoud, J. Faucher, D. Malec, and P. Maussion, Electrical Aging of the Insulation of Low-Voltage Machines: Model Definition and Test With the Design of Experiments, IEEE Trans. Ind. Electron., vol. 60, no. 9, pp. 4147,4155, Sep. 2013.

[16] I. T. T. C. Mil-dtl- and R. Hvh–dom, Remy s HVH410 Series. [Online]. Available: www.remyinc.com . [Accessed: 18-Oct-2014].

[17] O. Winter, C. Kral, and E. Schmidt, Augmented Temperature Degrading Effect of Rare Earth Magnets Arranged in Segmented Halbach Arrays, IEEE Trans. Magn., vol. 48, no. 11, pp. 3335,3338, Nov. 2012.

[18] M. Wi, Influence of d- and q -Axis Current on Demagnetization in PM Synchronous Machines, pp. 4380,4387, 2013.

[19] I. Semsei, On the nature of aging, Mech. Ageing Dev., vol. 117, pp. 93,108, 2000.

[20] I. Ali, A. Ginart, P. Kalgren, and M. Roemer, Actuator Remaining Life Estimation Under Fault Tolerant Operation, SAE Technical Paper 2010-01-1753, 2010.

https://dspace.org/

Cost functions for degradation control of electric motors in electric vehicles

Samaranayake, Lilantha; Longo, Stefano

2015-11-16
Institute of Electrical and Electronics Engineers (IEEE)
http://doi.org/10.1109/ECC.2015.7330617
Lilantha Samaranayake and Steano Longo. Cost functions for degradation control of electric motors in electric vehicles. European Control Conference, ECC 2015. 15-17 July 2015, Linz, Austria. pp660-665

Downloaded from a DSpace repository. https://dspace.org/